

Evidence for High-Frequency QPOs with a 3:2 Frequency Ratio from a 5000 Solar Mass Black Hole

Dheeraj R. Pasham^{1,2,3}, S. Bradley Cenko^{1,2,3}, Abderahmen Zoghbi^{4,5}, Richard F. Mushotzky^{1,3}, Jon Miller⁴, Francesco Tombesi^{1,2,3}

ABSTRACT

Following the discovery of 3:2 resonance quasi-periodic oscillations (QPOs) in M82X-1 (Pasham et al. 2014), we have constructed power density spectra (PDS) of all 15 (sufficiently long) *XMM-Newton* observations of the ultraluminous X-ray source NGC1313X-1 ($L_X \approx 2 \times 10^{40}$ erg/sec). We detect a strong QPO at a frequency of 0.29 ± 0.01 Hz in data obtained on 2012 December 16. Subsequent searching of all the remaining observations for a 3:2/2:3 frequency pair revealed a feature at 0.46 ± 0.02 Hz on 2003 Dec 13 (frequency ratio of 1.59 ± 0.09). The global significance of the 0.29 Hz feature considering all frequencies between 0.1 and 4 Hz is $> 3.5 \sigma$. The significance of the 0.46 ± 0.02 Hz QPO is $> 3.5 \sigma$ for a search at 2/3 and 3/2 of 0.29 Hz. We also detect lower frequency QPOs (32.9 ± 2.6 and 79.7 ± 1.2 mHz). All the QPOs are super-imposed on a continuum consisting of flat-topped, band-limited noise, breaking into a power-law at a frequency of 16 ± 3 mHz and white noise at $\gtrsim 0.1$ Hz. NGC1313X-1's PDS is analogous to stellar-mass black holes' (StMBHs) PDS in the so-called steep power-law state, but with the respective frequencies (both QPOs and break frequencies) scaled down by a factor of ~ 1000 . Using the inverse mass-to-high-frequency QPO scaling of StMBHs, we estimate NGC1313X-1's black hole mass to be $5000 \pm 1300 M_\odot$, consistent with an inference from the scaling of the break frequency. However, the implied Eddington ratio, $L_{Edd} > 0.03 \pm 0.01$, is significantly lower compared to StMBHs in the steep power-law state ($L_{Edd} \gtrsim 0.2$).

¹Astrophysics Science Division, NASA's Goddard Space Flight Center, Greenbelt, MD 20771; email: dheerajrangareddy.pasham@nasa.gov, brad.cenko@nasa.gov

²Astronomy Department, University of Maryland, College Park, MD 20742; email: ftombesi@astro.umd.edu; richard@astro.umd.edu

³Joint Space-Science Institute, University of Maryland, College Park, MD 20742, USA

⁴Department of Astronomy, University of Michigan, Ann Arbor, MI 48109-1042; email: abzoghbi@umich.edu; jonmm@umich.edu

⁵Cahill Center for Astrophysics, California Institute of Technology, Pasadena, CA 91125

Subject headings: X-rays: individual (NGC 1313 X-1) — X-rays: binaries — black hole physics — methods: data analysis

1. Introduction

Compact accreting X-ray sources in nearby galaxies with luminosities exceeding 10^{39} erg s^{-1} are referred to as ultraluminous X-ray sources (ULXs). Current evidence suggests that ULXs might be a mixed bag of compact objects including stellar-mass black holes (StMBHs: 3-25 M_{\odot}) powered by super-Eddington accretion (e.g., King et al. 2001, Begelman 2002, Gladstone et al. 2009), intermediate-mass black holes (IMBHs: a few \times (100-1000) M_{\odot} ; Kaaret et al. 2001, 2006, Matsumoto et al. 2001, Farrell et al. 2009, Pasham et al. 2014, Mezcua et al. 2015), and neutron stars (Bachetti et al. 2014).

One of the biggest challenges in understanding ULXs is to estimate their compact object masses. Because their optical counterparts are faint (V-band magnitudes of 22-24; e.g., Gladstone et al. 2013, Tao et al. 2011), Doppler tracking their optical counterparts to derive their mass functions—as done for Galactic StMBHs—has been extremely challenging (e.g., Roberts et al. 2011, Cseh et al. 2013). However, in a few ULXs, such optical measurements have yielded mass constraints that suggest lower-mass black holes ($\lesssim 30 M_{\odot}$; Liu et al. 2013, Motch et al. 2014).

It has been suggested that the detection of the 3:2 frequency ratio high-frequency quasi-periodic oscillations (QPOs) can resolve the ULX mass problem (Abramowicz et al. 2004). StMBH high-frequency QPOs (frequency range of 100-450 Hz; McClintock & Remillard 2006) that appear in a 3:2 frequency ratio scale inversely with the black hole mass. Moreover, it has been demonstrated that the power density spectra (PDS) of both the stellar-mass and the supermassive black holes are qualitatively similar. The PDS break timescale of both simply scale with the black hole mass, after accounting for the differences in the accretion efficiency between sources (e.g., McHardy et al. 2006, Kōrding et al. 2007). One can also use this break timescale to estimate black hole masses. Thus, under this black hole variability unification paradigm, 3:2 high-frequency QPO analogs of StMBHs should also be detectable from IMBHs, but with centroid frequencies scaled down according to their respective black hole masses (Vaughan & Uttley 2005). For example, a few 1000 M_{\odot} IMBH should exhibit high-frequency QPOs with centroid frequencies in the range of a fraction of Hz. In fact, such a 3:2 ratio QPOs have already been detected from the ULX M82 X-1. In that source, the two QPOs (3.3 and 5 Hz) allowed Pasham et al. (2014) to estimate its black hole mass to be $428 \pm 105 M_{\odot}$. Here, we report evidence for a second such high-frequency pair from another ULX, NGC 1313 X-1.

2. *XMM-Newton* Data

As of the writing of this paper, 22 of the 24 *XMM-Newton* observations of NGC 1313 are public. The three brightest X-ray sources in this field, the two ULXs, NGC 1313 X-1 (hereafter, X-1), X-2 and the X-ray bright supernova SN1978K are well separated in the XMM images (see Figure 1). Previous energy spectral studies of X-1 suggest it may host an IMBH with a mass of $\sim 1000 M_{\odot}$ (e.g., Miller et al. 2003, 2013). Given the frequency range we are interested in, we used data primarily from EPIC-pn, utilizing events in the entire 0.3-10.0 keV band pass. Both the pn and the MOS detectors were operated in the so-called full-frame mode during all the observations. While pn’s full-frame data mode offers a time resolution of 73.4 ms, i.e., Nyquist frequency of 6.82 Hz, MOS data is limited to a Nyquist frequency of only 0.19 Hz.

3. Analysis

We reduced all the observations using the standard data reduction procedures and removed datasets that were severely affected by background flaring. This preliminary screening left us with fifteen observations (Table 1). Source events were extracted from a circular region of radius $33''$ (dashed circle around X-1 in Figure 1) when X-1 was clear of a CCD gap. When X-1 was close to or on a CCD gap we extracted events from a smaller region of radius $25''$ excluding the CCD gap. Circular background regions of the same radius, and free of any point sources, were chosen away from the source’s readout column and as close to the telescope pointing as possible.

3.1. Results: Timing

In order to assess X-1’s variability, we first extracted the source and the background light curves from each of the fifteen observations. Background flaring was prominent for only brief durations in some observations. We constructed good time intervals (GTIs) accounting for both the background flares and times when the detector was turned off. Figure 2 contains sample background-subtracted X-ray light curves (black) and their respective backgrounds (red) from all the observations whose power spectra are described in this article.

Using the GTIs shown in Figure 2, we constructed a Leahy normalized (Poisson noise level of 2; Leahy 1983) PDS of X-1 from each of the individual observations. All the power spectra were sampled only up to 4 Hz, a value safely below the Nyquist frequency of 6.82 Hz, in order to avoid any aliasing affects. We started our timing analysis with the three

longest observations (obsIDs: 0405090101, 0693850501, and 0693851201) during which X-1 was positioned on-axis, giving the best sensitivity for detecting QPOs.

3.1.1. ObsID 0405090101

The top panel of Figure 3 shows the combined EPIC (pn+MOS) PDS from obsID 0405090101—sampled in the frequency range from 0.0022 to 4 Hz. We first extracted a pn-only PDS and found a QPO-like feature at 80 mHz, a frequency well below the MOS detectors’ Nyquist frequency. Therefore, in order to improve the signal, we used pn+MOS data in this single instance. It is evident that the overall shape of the power spectrum is flat-topped at the lowest frequencies, breaking into a power-law, and white noise at the highest frequencies. Two broad, QPO features at centroid frequencies of roughly 30 and 80 mHz are also apparent. We modeled the continuum with a constant plus a bending power law model¹ similar to other ULXs (e.g., Pasham & Strohmayer 2012, 2013), and StMBHs in the steep power-law state (McClintock & Remillard 2006). This gave a best-fit χ^2 of 419 for 252 degrees of freedom (dof). We then added a Lorentzian component to model the QPO at 80 mHz. This improved the χ^2 by 89, i.e., χ^2 of 330 for 249 dof. Using the F-test, this corresponds to a significance of 8×10^{-13} or $> 7\sigma$. The best-fit QPO has a centroid frequency, width, normalization, and a root-mean-squared (RMS) amplitude of 79.7 ± 1.2 mHz, 14.5 ± 3.4 mHz, 0.57 ± 0.09 , and $10.8 \pm 2.4\%$, respectively. Adding a second QPO improved the χ^2 by 40 (290 for 246 dof), which corresponds to an F-test probability of 6×10^{-7} ($> 4.9\sigma$). The best-fit centroid frequency, width, normalization and RMS amplitude of the second QPO were 32.9 ± 2.6 mHz, 18.2 ± 7.8 , 0.34 ± 0.08 , and $9.4 \pm 3.9\%$, respectively.

However, Protassov et al. (2002) pointed out the problems with applying the F-test in additive models. Therefore, in order to estimate the QPO significances independent of the F-test, we employed a rigorous Monte Carlo approach as follows.

1) We estimated the baseline bending power-law plus a constant model parameters along with their uncertainties, and then randomly sampled $N = 1.8 \times 10^6$ model parameter sets from within the best-fit parameter error bars (assuming normal distribution).

1

$$Power = C + \frac{N \times \nu^{-\alpha}}{\left[1 + \left(\frac{\nu}{\nu_{bend}} \right)^{\beta-\alpha} \right]}$$

where C , N , ν_{bend} are the Poisson noise level, the normalization of the bending power-law and the bending frequency, respectively while α and β are the power-law indices below and above the bending frequency, respectively.

2) For each of these parameter sets, we simulated a light curve of the same length as the observed one following the algorithm described in Timmer & Koenig (1995), and then extracted a PDS from this simulated light curve.

3) After binning these PDS in the same way as the original PDS, we modeled them with a bending power law. We then added a QPO to this model, with the QPO frequency constrained to lie between 0.01 and 1 Hz. The maximum improvement in χ^2 ($\Delta\chi_{max}^2$) was recorded from each simulated PDS.

4) The significance of the 80 mHz QPO was estimated as $1 - N_{(\Delta\chi_{max}^2 > \Delta\chi_{obs}^2)}/N$, where $N_{(\Delta\chi_{max}^2 > \Delta\chi_{obs}^2)}$ is the number of simulated $\Delta\chi_{max}^2$ values greater than the observed $\Delta\chi_{obs}^2$. For estimating the significance of the 30 mHz QPO, we assumed the baseline model to be the best-fit continuum plus 80 mHz QPO of the observed PDS, and recorded the maximum $\Delta\chi^2$ values by adding an additional QPO to this base model.

This methodology is similar to estimating the significances of spectral lines in energy spectra (e.g., Tombesi et al. 2010, Zoghbi et al. 2015). For the 80 mHz feature we ran 1.8×10^6 simulations. The maximum $\Delta\chi^2$ was 25, which is much lower than the observed value of 89. Thus, we conclude that the 80 mHz feature is significant at least at the 5σ level. We ran 200,000 simulations to test the significance of the 30 mHz feature and found that one run exceeded the observed $\Delta\chi^2$ of 40. Thus, we conclude its significance is $1 - (1/200,000)$ or $\approx 4.4\sigma$.

3.1.2. ObsID 0693850501

The PDS from observation 0693850501 exhibited a strong feature at roughly 0.3 Hz (bottom-left panel of Figure 3). The continuum looks flat because we only sampled up to roughly 0.02 Hz. A flat-topped, followed by a power-law like continuum can be seen when we sample up to 0.001 Hz using longer light curve segments. Modeling the continuum with a constant yielded a best-fit χ^2 of 186 for 127 dof. Adding a Lorentzian component improved the χ^2 by 56 with an addition of three parameters (χ^2 of 130 for 124 dof). This corresponds to an F-test probability of 1.1×10^{-9} or $> 6\sigma$. Using the Monte Carlo approach to test the significance, with 1.8×10^6 simulations, we find a lower limit of 5σ . For the Monte Carlo simulations, we modeled each of the simulated PDS with a constant, and a constant plus a Lorentzian model, and recorded the maximum improvement in the $\Delta\chi^2$. Out of the 1.8×10^6 simulations, the maximum $\Delta\chi^2$ improvement was 27, a value much less than the observed $\Delta\chi^2$ improvement of 56. The best-fit centroid frequency, width, normalization and the RMS of the QPO were 0.29 ± 0.01 Hz, 0.13 ± 0.04 Hz, 0.14 ± 0.03 , and $19.0 \pm 5.0\%$, respectively.

We also estimated the significance using another independent method. First we rescaled the PDS (rescaling factor of 1.01, and the rescaled power at 0.29 Hz—in the highest bin—is 2.173) so that the local mean around 0.5 Hz is equal to 2, the value expected from a purely Poisson (white noise) process. We then computed the probability with 3σ and the 4σ confidence, of obtaining a power that is at or higher than some threshold P_* , $\text{Probability}(P > P_*) = N_{\text{trials}} \times Q(P_* \times 898 \times 4 | 2 \times 898 \times 4)$, where $Q(P_* \times 898 \times 4 | 2 \times 898 \times 4)$ is the probability of obtaining a χ^2 value of $P_* \times 898 \times 4$ or higher from a χ^2 distribution with $2 \times 898 \times 4$ dof. We used this χ^2 distribution because we averaged in frequency by a factor of 4 and averaged 898 individual power spectra each derived from 128 s light curve segments. N_{trials} account for the total number of trials (frequency bins within 0.1-4 Hz). The confidence contours are marked by horizontal dotted lines in the bottom-left panel of Figure 3. Clearly, the highest bin in the 0.3 Hz QPO is significant at greater than the 4σ level.

After establishing the lower-frequency continuum and QPOs, and the 0.3 Hz QPO, we searched for a signal at $2/3$ and $3/2$ of 0.3 Hz separately from all the GTIs longer than 7 ks. The PDS from the 4^{th} GTI (exposure ≈ 22 ks) of this observation (top panel of Figure 4) showed evidence for excess power at 0.44 ± 0.06 Hz, a value consistent with $3/2$ of 0.3 Hz. This feature is significant at the 7.6×10^{-4} level (the significance is 1×10^{-2} if all frequencies were searched). We estimated the significance of this feature as follows. First, we estimated the probability of detecting a false peak with a power value of 2.13. This is the probability of getting a χ^2 value of $2.13 \times 174 \times 16$ or higher from a χ^2 distribution with $2 \times 174 \times 16$ dof. This value is 3.8×10^{-4} . However, after securing the 0.3 Hz feature, we searched in two bins, one at $2/3$ and the other at $3/2$ (bin width of 0.125 Hz). Considering the two trials, the significance in the 4^{th} GTI is $2 \times 3.8 \times 10^{-4}$. This significance level does not take into account the number of GTIs searched yet. We estimate its global significance—considering all GTIs—in section 3.1.5.

3.1.3. *ObsID 0693851201*

A feature at a frequency of 0.30 ± 0.02 Hz (middle panel of Figure 4) as observed in the PDS of observation 0693850501 (taken roughly a week before this observation) was again present, albeit at a lower significance of $\gtrsim 3.3\sigma$. Similar to the bottom-left panel of Figure 3, the dotted horizontal lines represent the 3 and the 4σ confidence contours considering all frequency bins (trials) between 0.1 and 4 Hz.

3.1.4. Other Observations

We then constructed PDS from each of the shorter observations. Observation 0150280401 showed evidence for a QPO with a centroid frequency of 0.46 ± 0.02 Hz (RMS amplitude of $12 \pm 2\%$), a value consistent with $3/2$ of 0.3 Hz. The significance of this feature—again considering a search around $2/3$ and $3/2$ of 0.3 Hz—is 2.8×10^{-4} estimated as follows. First, we estimated the probability of getting a power value of 2.451, i.e., the probability of getting a χ^2 value of $2.451 \times 81 \times 4$ or higher from a χ^2 distribution with $2 \times 81 \times 4$ dof. This value is 7×10^{-5} . However, considering that we searched in two bins (width per bin of 0.03125 Hz) around $3/2$ and $2/3$ of 0.3 Hz, this translates to $4 \times 7 \times 10^{-5}$ ($> 3.5\sigma$). The significance of the feature considering a full frequency search is 6×10^{-3} .

Observation 0205230601 showed weak evidence for QPO-like feature at the $> 2\sigma$ level (Bottom panel of Figure 4). The PDS from the remaining observations were essentially featureless with evidence for red-noise in a handful of them. To ensure that these QPO features are not associated with the background, we extracted all the background PDS from these fifteen observations. They are all consistent with being featureless (flat, white noise) within the error bars.

3.1.5. Global probability of the 0.45 and the 0.3 Hz QPOs

In order to estimate the global significance of the 0.45 Hz QPO we considered all the 24 GTIs—longer than 7 ks—where we searched for QPOs (see Table 1). Figures 3 & 4 show all the statistically significant QPOs detected during this search. The QPO’s global probability can be calculated straightforwardly using the binomial distribution formula which gives the probability of happening of a certain event m times in n trials as,

$$P(m; p, n) = \frac{n!}{m!(n-m)!} p^m (1-p)^{n-m}$$

where n is the total number of GTIs searched, and m is the number of GTIs where the signal was detected at a probability of p .

Using the above formula, the global probability of detecting the 0.45 Hz feature at $> 7.6 \times 10^{-4}$ significance in two (m) out of the twenty four (n) GTIs is 1.6×10^{-4} ($> 3.5\sigma$).

Similarly, we estimate the global probability of the 0.3 Hz QPO, using $n = 24$, $m = 1$, and $p = 5.6 \times 10^{-7}$ (5σ), to be $> 3.5\sigma$. *Note that this is very conservative lower limit as we have not included the case where the 0.3 Hz feature was detected at $> 3.3\sigma$.*

4. Discussion

NGC 1313 X-1’s PDS has all the features of a typical StMBH in the steep power-law state, but with characteristic time scales $\sim 1000\times$ longer. Typical StMBHs have three components: (1) A continuum often flat-topped at the lowest frequencies, with a power-law like decline beyond a certain break frequency, followed by white noise at the highest frequencies; (2) Low-frequency QPOs (frequencies of a few Hz); and, finally (3) High-frequency QPOs (frequency range of 100-450 Hz) exhibited by some systems. Three StMBHs with known masses show high-frequency QPOs in harmonic pairs with centroid frequencies in a ratio consistent with 3:2 (e.g., Miller et al. 2001, Strohmayer et al. 2001a, 2001b, Remillard et al. 2002). In these systems, the two QPOs are often not simultaneous (e.g., see Table 1 of Remillard 2002 & Strohmayer 2001b). Furthermore, unlike the low-frequency QPOs, these are stable in frequency with changes in source luminosity (McClintock & Remillard 2006). Also, the timescales associated with them (~ 0.01 s) are comparable to the Keplerian orbital periods of a test particle close to the innermost stable circular orbit. The commonalities of the high-frequency QPOs in these three StMBH systems suggests a common physical origin. Under the assumption that these originate from a radius fixed in gravitational units (GM/c^2 , where G , M , and c are the Gravitational constant, the black hole mass and the speed of light, respectively), their frequency should simply scale inversely with the black hole mass. Indeed, the three StMBHs with high-frequency QPOs do agree with this inverse scaling law (see Figure 4.17 of McClintock & Remillard 2006, Zhou et al. 2015).

We suggest that the observed lower 30 and 80 mHz, and the higher 0.3 and 0.45 Hz 3:2 ratio QPOs are the analogs of the low and the high-frequency QPOs of StMBHs, and that X-1 may be in an X-ray accretion state similar to the steep power-law state of StMBHs. This result agrees with prior work by Feng & Kaaret (2006), who studied X-1’s X-ray (0.3-10 keV) energy spectral variability using *XMM-Newton* data taken between 2000 and 2005. They concluded that the source resides in either the steep power-law state—at high luminosities—or in the low/hard state at lower luminosities, but never enters the thermal dominant state (see Bachetti et al. 2013 for alternate arguments).

Using the dynamical masses and the high-frequency QPOs of StMBHs² XTE J1550-564, GRO J1655-50, and GRS 1915+105, we estimate—based on the inverse mass scaling—that X-1’s black hole mass is $5000\pm 1300 M_{\odot}$. We also measured the mass using the break frequency–black hole mass-accretion rate scaling as derived by McHardy et al. (2006). Using

²XTE J1550-564, GRO J1655-50 and GRS 1915+105 have high-frequency QPOs at 184 & 276 Hz, 300 & 450 Hz, and 113 & 168 Hz, respectively. Their black hole masses are $9.1\pm 0.61 M_{\odot}$ (Orosz et al. 2011), $5.4\pm 0.3 M_{\odot}$ (Beer & Podsiadlowski 2002), and $10.1\pm 0.6 M_{\odot}$ (Steehgs et al. 2013), respectively.

a break frequency of 16 ± 3 mHz from obsID 0405090101, and assuming a lower limit on the bolometric luminosity of 2×10^{40} erg s $^{-1}$ implies a black hole mass of $> 7600\pm 5600 M_{\odot}$ ³. This value is consistent with the measurement from the 3:2 QPO pair.

Yang et al. (2011) estimated X-1’s bolometric correction factor (ratio of the X-ray-to-Optical flux) to be similar to that of typical StMBHs, implying that a significant fraction of the emission is in the X-rays. X-1’s average X-ray (0.3-10.0 keV) luminosity of 2×10^{40} erg s $^{-1}$ (e.g., Feng & Kaaret 2006) implies an Eddington ratio of $> 0.03\pm 0.01$. This value is significantly low compared to the typical Eddington ratios of StMBHs in the steep power-law state ($> 0.2L_{Edd}$; McClintock & Remillard et al. 2006). Assuming the 0.2 value reported by McClintock & Remillard (2006), X-1’s low Eddington ratio is inconsistent with the interpretation of it being in the steep power-law state.

Bachetti et al. (2013) carried out timing analysis of two of the data sets described here (0693850501 and 0693851201). However, they did not report any evidence for QPOs at 0.3 Hz. We suspect the reason for this discrepancy is because they extracted their PDS using both the pn and the MOS data. As described earlier, MOS is limited to a frequency of ≈ 0.19 Hz. In addition to any signal beyond 0.19 Hz being unreliable, even at frequencies lower than, but close to 0.19 Hz, signal suppression can be severe (van der Klis 1989). To test this, we extracted a PDS using a combined pn and MOS event list from the observations 0693850501 and 0693851201. While we still see evidence for a feature at 0.3 Hz and at ~ 90 mHz, they were statistically less significant than in the analysis presented above.

The first ULX 3:2 pair from M82 X-1 was detected using the Rossi X-ray Timing Explorer (*RXTE*), while the detection reported here is from *XMM-Newton*. Currently, *XMM-Newton* is the only X-ray observatory that can provide both large enough effective area and the required time resolution to detect these oscillations from ULXs. Therefore, deeper X-ray observations of other variable ULXs, *viz.*, NGC 5408 X-1 (Middleton et al. 2011), NGC 6946 X-1 (Rao et al. 2010) are strongly encouraged. Also, the reported 3:2 pair from X-1 boosts confidence in the prospects of detecting high-frequency QPOs from relatively isolated ULXs with Neutron star Interior Composition ExploreR (*NICER*)—with an anticipated effective area of 1.5 times greater than EPIC-pn.

Acknowledgements: We thank the referee for his/her valuable comments/suggestions that improved the paper.

³The high uncertainty from the break frequency scaling is due to large error bars on the coefficients of the scaling law; See Figure 1 of McHardy et al. (2006).

REFERENCES

- Abramowicz, M. A., Kluźniak, W., McClintock, J. E., & Remillard, R. A. 2004, *ApJ*, 609, L63
- Abramowicz, M. A., & Kluźniak, W. 2004, *X-ray Timing 2003: Rossi and Beyond*, 714, 21
- Bachetti, M., Rana, V., Walton, D. J., et al. 2013, *ApJ*, 778, 163
- Bachetti, M., Harrison, F. A., Walton, D. J., et al. 2014, *Nature*, 514, 202
- Beer, M. E., & Podsiadlowski, P. 2002, *MNRAS*, 331, 351
- Begelman, M. C. 2002, *ApJ*, 568, L97
- Belloni, T. M., Sanna, A., & Méndez, M. 2012, *MNRAS*, 426, 1701
- Cseh, D., Gris e, F., Kaaret, P., et al. 2013, *MNRAS*, 435, 2896
- Dheeraj, P. R., & Strohmayer, T. E. 2012, *ApJ*, 753, 139
- Farrell, S. A., Webb, N. A., Barret, D., Godet, O., & Rodrigues, J. M. 2009, *Nature*, 460, 73
- Feng, H., & Kaaret, P. 2006, *ApJ*, 650, L75
- Gladstone, J. C., Roberts, T. P., & Done, C. 2009, *MNRAS*, 397, 1836
- Gladstone, J. C., Copperwheat, C., Heinke, C. O., et al. 2013, *ApJS*, 206, 14
- Kaaret, P., Prestwich, A. H., Zezas, A., et al. 2001, *MNRAS*, 321, L29
- Kaaret, P., Simet, M. G., & Lang, C. C. 2006, *Science*, 311, 491
- King, A. R., Davies, M. B., Ward, M. J., Fabbiano, G., & Elvis, M. 2001, *ApJ*, 552, L109
- K rding, E. G., Migliari, S., Fender, R., Belloni, T., Knigge, C., & McHardy, I. 2007, *MNRAS*, 380, 301
- Leahy, D. A., Darbro, W., Elsner, R. F., et al. 1983, *ApJ*, 266, 160
- Liu, J.-F., Bregman, J. N., Bai, Y., Justham, S., & Crowther, P. 2013, *Nature*, 503, 500
- Matsumoto, H., Tsuru, T. G., Koyama, K., et al. 2001, *ApJ*, 547, L25
- McClintock, J. E., & Remillard, R. A. 2006, *Compact stellar X-ray sources*, 157

- McHardy, I. M., Koerding, E., Knigge, C., Uttley, P., & Fender, R. P. 2006, *Nature*, 444, 730
- Mezcua, M., Roberts, T. P., Lobanov, A. P., & Sutton, A. D. 2015, *MNRAS*, 448, 1893
- Miller, J. M., Wijnands, R., Homan, J., et al. 2001, *ApJ*, 563, 928
- Miller, J. M., Fabbiano, G., Miller, M. C., & Fabian, A. C. 2003, *ApJ*, 585, L37
- Miller, J. M., Fabian, A. C., & Miller, M. C. 2004, *ApJ*, 614, L117
- Miller, J. M., Walton, D. J., King, A. L., et al. 2013, *ApJ*, 776, L36
- Motch, C., Pakull, M. W., Soria, R., Grisé, F., & Pietrzyński, G. 2014, *Nature*, 514, 198
- Orosz, J. A., Steiner, J. F., McClintock, J. E., et al. 2011, *ApJ*, 730, 75
- Pasham, D. R., & Strohmayer, T. E. 2013, *ApJ*, 771, 101
- Pasham, D. R., Strohmayer, T. E., & Mushotzky, R. F. 2014, *Nature*, 513, 74
- Protassov, R., van Dyk, D. A., Connors, A., Kashyap, V. L., & Siemiginowska, A. 2002, *ApJ*, 571, 545
- Remillard, R. A., Muno, M. P., McClintock, J. E., & Orosz, J. A. 2002a, *ApJ*, 580, 1030
- Remillard, R. A., McClintock, J. E., Orosz, J. A., & Levine, A. M. 2006, *ApJ*, 637, 1002
- Roberts, T. P., Gladstone, J. C., Goulding, A. D., et al. 2011, *Astronomische Nachrichten*, 332, 398
- Ryder, S. D., Staveley-Smith, L., Malin, D., & Walsh, W. 1995, *AJ*, 109, 1592
- Steehls, D., McClintock, J. E., Parsons, S. G., et al. 2013, *ApJ*, 768, 185
- Strohmayer, T. E. 2001a, *ApJ*, 552, L49
- Strohmayer, T. E. 2001b, *ApJ*, 554, L169
- Tao, L., Feng, H., Grisé, F., & Kaaret, P. 2011, *ApJ*, 737, 81
- Timmer, J., & Koenig, M. 1995, *A&A*, 300, 707
- Tombesi, F., Cappi, M., Reeves, J. N., et al. 2010, *A&A*, 521, A57
- van der Klis, M. 1989, *Timing Neutron Stars*, 27

Vaughan, S., & Uttley, P. 2005, MNRAS, 362, 235

Yang, L., Feng, H., & Kaaret, P. 2011, ApJ, 733, 118

Zhou, X.-L., Yuan, W., Pan, H.-W., & Liu, Z. 2015, ApJ, 798, L5

Zoghbi, A., Miller, J. M., Walton, D. J., et al. 2015, ApJ, 799, L24

Table 1: Summary of the *XMM-Newton* observations of NGC 1313 X-1

ObsID	Date (UTC) ¹	Observation Time (ks) ²	Count rate ³ (counts s ⁻¹)	Effective Exposure ⁴ (ks)	Number of GTIs > 7 ks
0106860101	2000-10-17	42.4	0.73 ± 0.005	31.6	1
0150280301	2003-12-21	16.2	1.02 ± 0.01	9.7	1
0150280401	2003-12-23	20.9	0.91 ± 0.008	10.5	1
0150280501	2003-12-25	21.4	0.70 ± 0.007	9.8	1
0150280601	2004-01-08	53.2	0.79 ± 0.007	12.4	1
0150281101	2004-01-16	8.9	0.87 ± 0.01	7.0	1
0205230301	2004-06-05	11.9	1.27 ± 0.01	10.0	1
0205230401	2004-08-23	18.0	0.63 ± 0.006	14.9	1
0205230501	2004-11-23	16.0	0.26 ± 0.004	14.0	1
0205230601	2005-02-07	14.3	0.57 ± 0.007	12.4	1
0301860101	2006-03-06	21.8	1.11 ± 0.008	19.9	1
0405090101	2006-10-15	123.1	0.70 ± 0.002	121.1	3
0693850501	2012-12-16	125.2	0.83 ± 0.003	123.0	4
0693851201	2012-12-22	125.2	0.85 ± 0.003	123.0	4
0722650101	2013-06-08	30.7	0.71 ± 0.005	28.8	2

¹

Coordinated Universal Time. ² Total observation time in ks. ³ Average EPIC-pn 0.3-10 keV count rate of NGC 1313 X-1. Note, however, that X-1 was not always on-axis. ⁴ After accounting for flaring background and instrumental good time intervals.

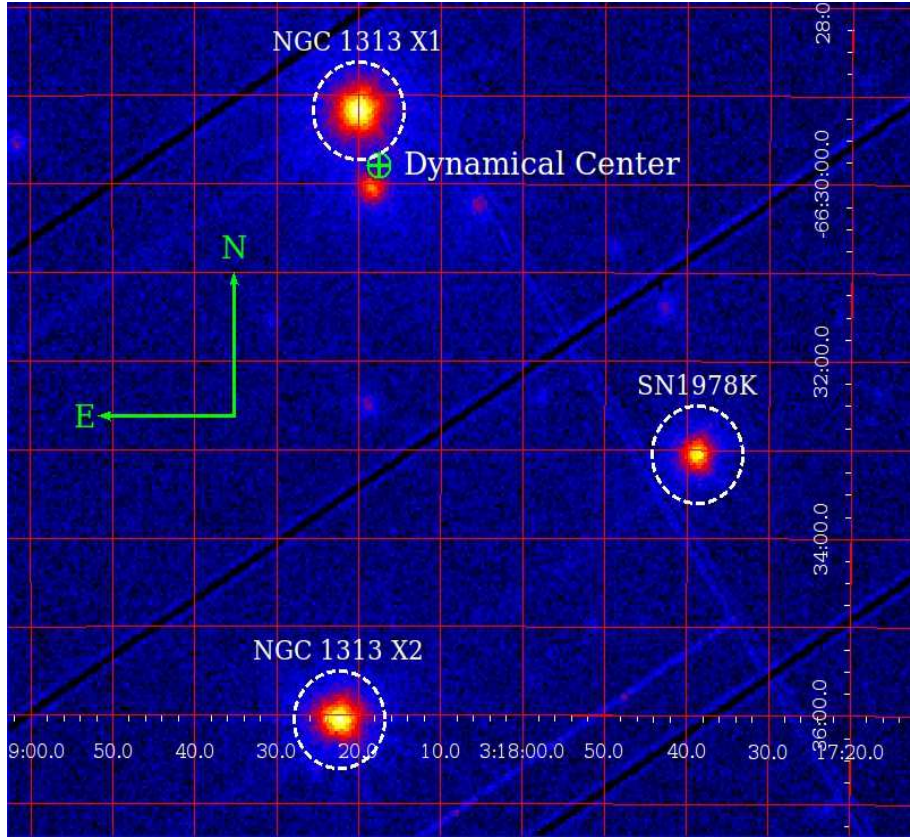


Figure 1: *XMM-Newton*/EPIC-pn X-ray (0.3-10 keV) image of NGC 1313, from observation 0693850501, produced with DS9. The dashed circles have a radius of $33''$ and indicate the size of our typical source extraction region. The dynamical center of the host galaxy, shown as an encircled cross, is based on H I maps by Ryder et al. (1995). The north and the east arrows are each $100''$ long.

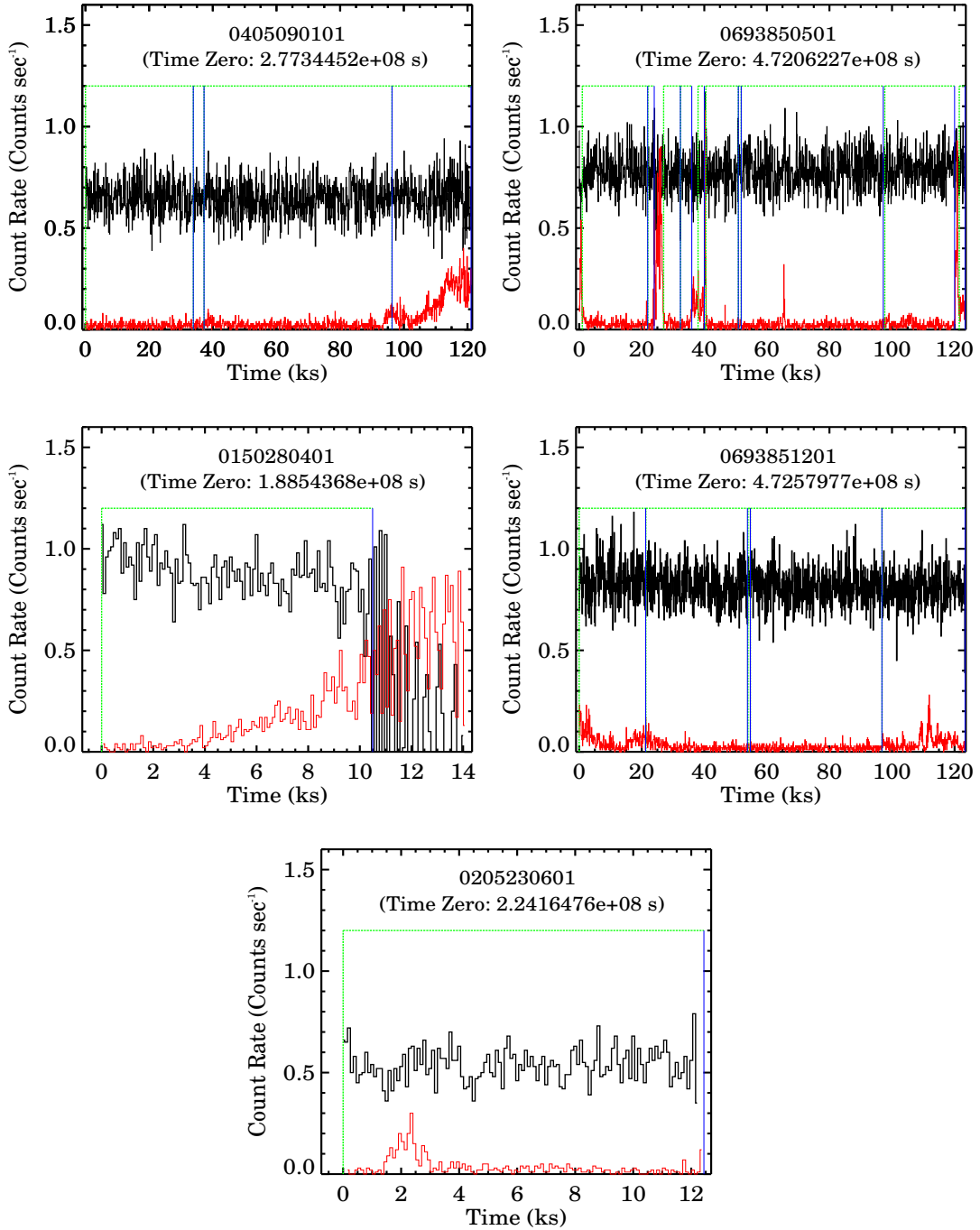


Figure 2: Background-subtracted EPIC-pn X-ray (0.3-10 keV) light curves of NGC 1313 X-1 (black), and their backgrounds (red) during five different *XMM-Newton* observations. The PDS from these data sets are shown in Figures 3 & 4. For each panel, their observation ID and time zero in seconds since 1998.0 TT are indicated at the top. Also shown are the good time intervals (GTIs) with duration longer than 500 s. A dashed vertical green line and a solid vertical blue line mark the beginning and end of a GTI, respectively.

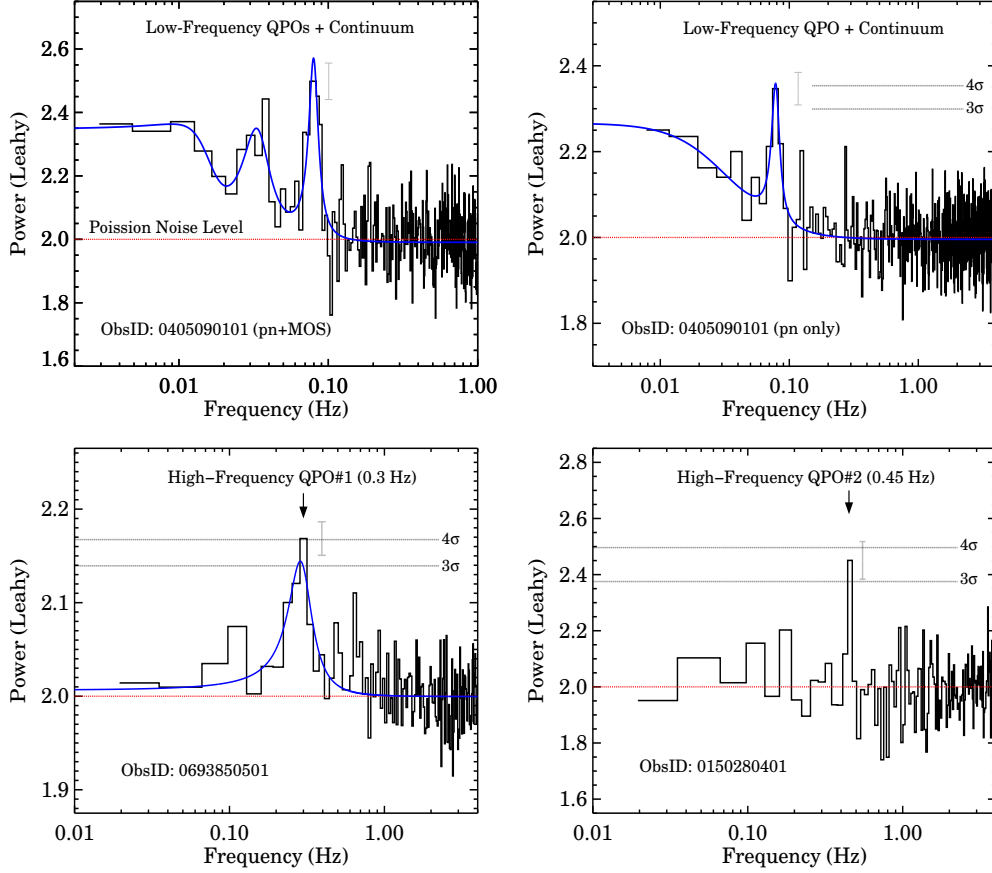


Figure 3: *XMM-Newton*/EPIC (0.3–10.0 keV) power density spectra of NGC 1313 X-1 from three different observations. **Top Left Panel:** pn+MOS PDS from observation 0405090101 (frequency resolution of 3.9×10^{-3} Hz). The continuum was modeled with a constant plus a bending power-law, while the QPOs at 30 mHz (Q value: $\nu/\Delta\nu \approx 2$) and 80 mHz (Q value ≈ 5.5) were modeled with Lorentzians. The solid blue line is the best-fit model. The PDS was obtained by averaging 235 PDS constructed from 512 s light curve segments binned at 1/8 s. **Top Right Panel:** pn only PDS from observation 0405090101 (frequency resolution of 7.8×10^{-3} Hz). The 3 and the 4σ contours for $\gtrsim 0.1$ Hz (considering all frequency bins between 0.1 and 4 Hz), and the best-fit bending power-law model with a QPO (blue) are also shown. **Bottom Left Panel:** EPIC-pn PDS (frequency resolution of 0.03125 Hz) from observation 0693850501 showing a strong QPO feature at 0.29 ± 0.01 Hz (Q value = 2.2). Also shown are the 3 and the 4σ significance contours considering all the frequency bins (trials) within 0.1 and 4 Hz of this observation. While the F-test suggests a significance of $> 6\sigma$, full Monte Carlo simulations imply a lower limit of 5σ . **Bottom Right Panel:** EPIC-pn PDS from observation 0150280401 showing a power spectral feature at 0.46 ± 0.02 Hz (Q > 14), consistent with 3/2 of 0.29 Hz. This PDS was constructed from 128 s segments binned at 1/8 s. The 3 and the 4σ contours take into account 4 bins (2 at 3/2 and 2/3 of 0.3 Hz and each 0.03125 Hz wide). In all the three cases, the Poisson noise level is marked by a dashed red line and the 1σ error bars of the highest bins of the QPOs are indicated in gray.

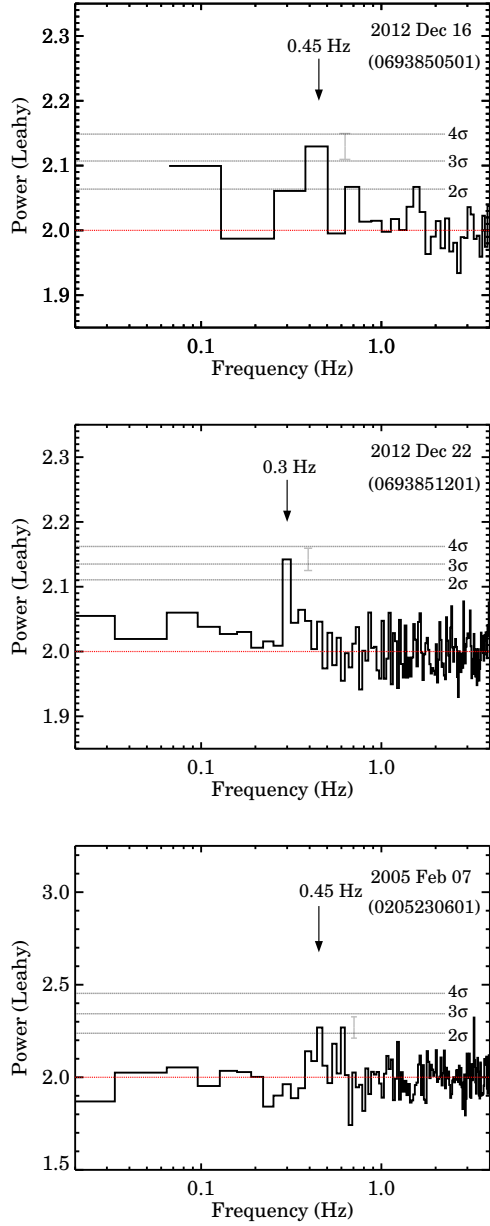


Figure 4: EPIC-pn (0.3–10.0 keV) power spectra of NGC 1313 X-1 from observations 0693850501 (top: using only the last GTI of ≈ 22 ks), 0693851201 (middle), and 0205230601 (bottom). These show epochs—in addition to those shown in Figure 3—with excess power around 0.3 and 0.45 Hz. The frequency resolution in the top, middle and the bottom PDS is 0.125, 0.03125 and 0.03125 Hz, respectively. The top PDS was constructed from 128 s light curve segments while the middle and the bottom were constructed from 256 s light curve segments binned at 1/8 s. The number of PDS averaged in the top, middle and the bottom panels were 174, 478, and 48, respectively. The confidence contours (estimated for a given observation and are not global; see 3.1.5 for global significances) in the top and the bottom panels take into account two, and four frequency bins, respectively (see text), while the contours in the middle panel take all the frequency bins between 0.1 and 4 Hz into account.